Comput Mech
DOI 10.1007/s00466-007-0164-z

ORIGINAL PAPER

Detection of stiffness degradation in laminated composite plates by filtered noisy impact testing

Sang-Youl Lee · Guillermo Rus · Taehyo Park

Received: 18 January 2006 / Accepted: 25 January 2007

Abstract The purpose of this paper is to detect damage (stiffness degradation) of laminated composite plates from noisy impact response data. The combined finite element method (FEM) with five degrees of freedom (DOF) and the advanced noise filtering algorithm described in this paper may allow us not only to detect the deteriorated elements but also to find their locations and the extents. A first order shear deformation theory (FSDT) is used to predict the structural behavior and to detect damage of laminated composite plates. The filtering procedure is designed by means of a wavelet decomposition together with a selection of the measuring points, and the optimization criterion is constructed on an estimate of the probability of detection using genetic algorithms. All these techniques are applied for the first time to composites. The effects of filtered noise associated with the uncertainty of measurements due to the complex nature of composites are considered for different layup sequences, number of layers, and length–thickness ratios. Several numerical results show that the noise filtering system is computationally efficient in identifying stiffness degradation for complex structures such as laminated composites.

S. -Y. Lee · T. Park
Department of Civil Engineering,
Hanyang University, Seoul 133-791, South Korea
e-mail: leesy72@hanyang.ac.kr

T. Park
e-mail: cepark@hanyang.ac.kr

G. Rus (✉)
Department of Structural Mechanics,
University of Granada, Granada 18071, Spain
e-mail: grus@ugr.es

Keywords Composite plate · Inverse problem · Impact testing · Wavelet analysis · Noise filter · Finite element method

1 Introduction

Advanced composite materials are attractive for use in various engineering applications due to their high strength-to-weight and stiffness-to-weight ratios, corrosion resistance, light weight and potentially high durability. The mechanical behaviors of composite structures with damages are complicated and difficult to analyze for different layup sequences. Structural behavior of laminated composite plates with or without damages has been studied previously by a host of investigators using a variety of approaches [9,12,13,21,23]. These works, based on forward problems, produce specific responses from known damaged extent and location.

Recently, some investigators started turning their attention to the damage detection by solving the inverse problem from static or dynamic responses obtained by the forward procedure. Direct search methods, such as neural networks, genetic algorithms and simulated annealing methods are developed and promisingly applied to the field of structural identification. Among them, genetic algorithms (GA) attract our attention because of the fact that the technique requires significantly small amount of data in dealing with complex problems, while attaining global convergence as opposed to gradient-based methods. Suh et al. [27] presented a hybrid neuro-genetic technique that is able to identify the location and extent of damage in a beam or frame structure using only the frequency information. Mares

and Surace [19] demonstrated the ability of the GA to identify damage in elastic structures. Friswell et al. [5] combined the genetic and eigen-sensitivity algorithms for locating damage. Chou and Ghaboussi [4] proposed a GA-based method to determine the location and extent of damage in truss structures from the measured static displacements. Krawczuk [11] presented a wave propagation approach to detect damage in beam structures based on GA and a gradient-based technique. However, all these works are limited in that they can analyze only structural members made of isotropic materials. Recently, techniques for detecting damages from noisy static or dynamic responses of anisotropic plates are evolving. Lee and Wooh [15] applied an advanced micro-genetic algorithm for detecting damage of steel and composite structures subjected to dynamic loading. Rus et al. [26] dealt with a method of damage detection for plane stress problem of composites using boundary element method (BEM). Lee and Wooh [14] applied the micro-genetic algorithm for detecting stiffness reduction of composite plates based on the high order shear deformation theory (HSDT).

Despite the broad spectrum of applications for detecting damage, the numerical techniques may not be attractive from the practical point of view. The methods require a precise measurement of static or impact loading to the structure that needs to be input into the numerical model. Based on experimental work, precise control and measurement of input loading are extremely difficult because of errors (noisy responses) arising from structures. In order to solve the inverse problem of composite structure with noisy data, the conventional techniques usually require a large number of iterations, and thus, a high computational cost. Therefore, an effective reduction of the noise may be significant issue for faster convergence, better computational efficiency and more precise and sensitive detection.

In order to reduce the noise effect in the dynamic response data, this study is focused on an efficient filtering algorithm based on the wavelet transform. The wavelet transform is a technique for the processing of signals whose spectral countenance is non-stationary. It is defined in terms of a base function, and obtained by compression, dilatation and decay operations of the mother wavelet. In the wavelet transform, the signal spectrum is divided by an overlapping of pass band filters with constant relative bandwidth. Addison [1] gives an excellent overview of the potential that the novel wavelet analysis provides to different areas of science in the current days. Within the subject of mechanical systems, Kim [10] gives a successful wavelet ridge analysis of the correlation of reflected to incident wave magnitude ratio over the time and frequency to correlate an experiment with a bending beam model. This application is merged with numerical methods by Li et al. [17] who use the wavelet finite element method (WFEM) in modal analysis to find cracks with the aim of solving accurately the crack singularities. On the other hand, wavelets can also be used for noise removal, which is our objective in this study. Messina et al. [20] compares wavelets for noise removal against differentiator filters, concluding that they provide similar performance. In a similar approach, Yang et al. [29] apply envelope complex wavelet analysis correlation to efficiently discriminate noise from the signals in an experimental case. In this study, a standard wavelet analysis is used as a filtering tool within a novel framework of optimization of the search methodology.

In standard practice of nondestructive evaluation (NDE), the issue of the probability of detection (POD) has only been addressed independently, under the name of identifiability, in statistics and mathematics, with a wide application in chemistry and physics. However, in the field of nondestructive testing, only observational comments have been made. Only Liu et al. [18] discussed as identifiability the relationship between the number of measurements and the number of degrees of freedom to establish a necessity condition. Tarantola et al. [28] examined the inversion theory under a probabilistic formulation and introduced probability density functions in the model and the a priori information about the parameters to explain the robustness of the inversion and to obtain a non-single valued output for the parameters. In this study, an estimate of the POD is designed from the minimization search approach as a criteria to be optimized for the design of the formulation.

The forward and inverse procedures are presented for the identification of stiffness degradation in laminated composite plates by combining the FEM as the numerical procedure for the simulation of the effect of the defect on the response to impact loading, and a parameterization of the defect in combination with a calibrating cost functional that incorporates an optimized noise filter. A standard GA is used for the optimization and search procedures. In this study, an efficient method to identify stiffness degradation in structures is proposed by combining GA with a filter for noisy dynamic response. This filter weights the wavelet coefficients, time windows and measurement points. Then, the POD is approximated from certain simulated values of the measurements. Finally, the proposed method determines the best measuring points, wavelets levels and time windows for locating and evaluating stiffness degradation on composite plates. This is tested for several combinations of layup sequences, number of layers, and length-thickness ratios.

2 Forward procedure

2.1 FEM model with degraded element

In order to measure the dynamic data from the degraded composite structure, the FEM is implemented to simulate the forward procedure. In a finite element formulation for solving a forward problem, the stiffness matrix of a structural system is expressed in terms of its material properties, geometry, and boundary conditions. Although it is not the limitation of the approach for composites in general (e.g. delaminations), we have a limited study scope in this paper, in that the damage (degradation) is defined as the stiffness reduction factor $\beta^{(m)}$ at one or more local areas [19,2,15]. This definition makes the described procedure applicable to stiffness reduction types of damage, and therefore excludes delamination types. Those defects can be tackled using the presented methodology by adapting the FEM damage model and the experimental design accordingly. Figure 1 shows the geometry of a composite plate with the degraded element. In specific, the structure is discreted into a set of finite elements categorized into undamaged and damaged states in different degradation levels. For such a plate model using the FSDT, the 8×8 global stiffness matrix of the mth damaged element can be expressed in the form

$$\tilde{\mathbf{C}}^{(m)} = \beta^{(m)}\mathbf{C}^{(m)} = \beta^{(m)} \begin{bmatrix} \mathbf{A} & \mathbf{B} & 0 \\ \mathbf{B} & \mathbf{D} & 0 \\ 0 & 0 & \mathbf{A} \end{bmatrix}, \tag{1}$$

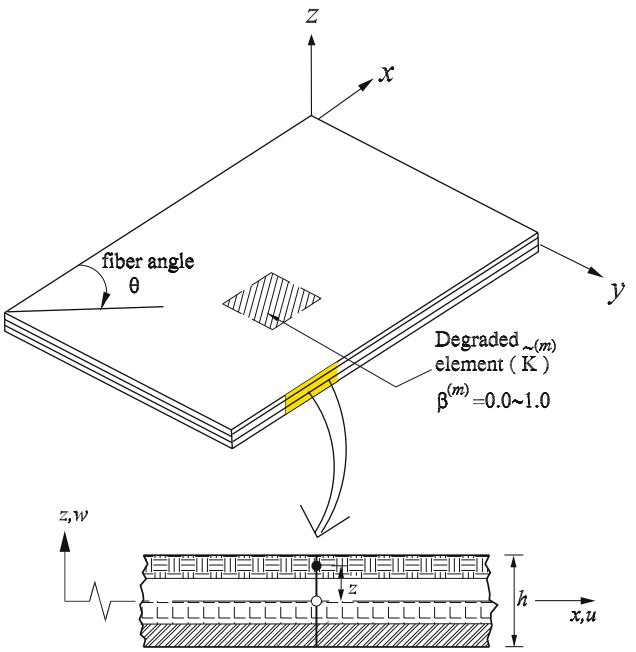

Fig. 1 Geometry of a composite plate with degraded element

where

$$(A_{ij}, B_{ij}, D_{ij}) = \sum_{k=1}^{n} \int_{z_k}^{z_{k+1}} \bar{Q}_{ij}^{(k)}(1, z, z^2)dz, \quad i,j = 1,2,6 \tag{2}$$

$$A_{ij} = \sum_{k=1}^{n} \int_{z_k}^{z_{k+1}} \bar{Q}_{ij}^{(k)}dz, \quad i,j = 4,5, \tag{3}$$

where, $\bar{Q}_{ij}^{(k)}$ denotes the stiffnesses of the kth layer whose top and bottom face positions are denoted by z_{k+1} and z_k, respectively. The laminate is made of several layers, with their material axes oriented arbitrarily with respect to the laminate coordinates, the constitutive equations of each layer must be transformed to the laminate coordinates. In Eqs. (2) and (3), the stiffnesses $\bar{Q}_{ij}^{(k)}$ mean the stress–strain relations when transformed to the laminate coordinates. In Eq. (1), $\mathbf{C}^{(m)}$ represents the stiffness in its virgin (undamaged) state. The tilde symbol placed above a variable is used to denote the damaged state. Notice that the coupling term B_{ij} disappears in the case of symmetric laminates [16]. The stiffness matrix of the damaged element in the local coordinates can now be written as the volume integral of the form

$$\tilde{\mathbf{K}}^{(m)} = \beta^{(m)} \int_V \mathbf{B}^{(e)T}\tilde{\mathbf{C}}^{(m)}\mathbf{B}^{(e)}d\Omega, \tag{4}$$

where $\mathbf{B}^{(e)}$ is the strain-displacement matrix of the element e, and the superscript T denotes the transpose operator. Note that $\mathbf{B}^{(e)}$ is a property that is independent of damage, thus it is applicable to all the elements e, whether damaged or undamaged. The governing equations of motion for the system is written in the form

$$\mathbf{M}\ddot{\mathbf{u}} + \mathbf{K}\mathbf{u} = \mathbf{r}, \tag{5}$$

where $\mathbf{u}$ and $\ddot{\mathbf{u}}$ are the displacement and acceleration vectors, $\mathbf{M}$ and $\mathbf{K}$ are the mass and stiffness matrices and $\mathbf{r}$ is the time history of the applied load, respectively. The damping effects in Eq. (5) are neglected, because the damping matrix can not be constructed from element damping matrices, such as the mass and stiffness matrices of the element assemblage [3].

To advance the solution of this equation in time, we use Newmark's direct integration method [3], in which the time dimension is represented by a set of discrete points with time increment of Δt. In other words, the value of a function $\xi(t)$ at time $t = n\Delta t$ is denoted by the index n as

$$\xi(t) = \xi(n\Delta t) = \xi[n], \quad n = 0, \ldots, N, \tag{6}$$

where $N+1$ is the total number of temporal discretization points for the entire duration of time T_d:

$$N = \text{int}\left(\frac{T_d}{\Delta t}\right) + 1\,. \tag{7}$$

At a given time step $t = n\Delta t$, the displacements of the damaged structure evaluated at the increased time $t = (n+1)\Delta t$ can be expressed as

$$\mathbf{u}[n+1] = [\hat{\mathbf{r}}[n+1] + \mathbf{M}(\lambda_0\mathbf{u}[n] + \lambda_2\dot{\mathbf{u}}[n] + \lambda_3\ddot{\mathbf{u}}[n])] \times [\hat{\mathbf{K}} + \lambda_0\mathbf{M}]^{-1}\,, \tag{8}$$

where $\hat{\mathbf{r}}$ is effective loads at the increased time $t = (n+1)\Delta t$, $\hat{\mathbf{K}}$ is the triangularized system stiffness matrix, $\dot{\mathbf{u}}$ is the velocity vector, and λ_0, λ_2, and λ_3 are the time integration constants at time t for the Newmark's method, respectively. It is possible to express Eq. (8) in terms of not only the displacements but also the other parameters such as velocity, acceleration or strain.

2.2 Noise effect

In order to consider unexpected errors in the measured displacements or accelerations, the usual option is to introduce the effects of random noise by adding Gaussian noise directly to the values computed by the FEM. Given a measured response on the kth node, a Gaussian (Normal) random number generator is used to generate a series of random numbers $\zeta_k[n]$ with standard deviation $\sigma = 1$ and zero mean. This series simulates a random process $\zeta(t)$, and the simulated measurements are given by,

$$\psi^x(\mathbf{p};\sigma_n)[n] \simeq \psi(\mathbf{p})[n] + h(n) * RMS(\psi)\zeta[n] \tag{9}$$

where $h(n)$ is the time-discretized Fourier transform of the frequency spectrum $H(\omega_j)$ of the noise, $*$ stands for convolution product and *RMS* stands for the root mean square value. The response is ultimately dependent on two variables: the parameters $\mathbf{p}$ that describe the defect, and are explained in detail in Sect. 3.1, and the standard deviation of the noise σ_n, where n stands for *noise*. In the following numerical experiments, only white noise (uniform frequency spectrum) is used, but in case the process is assigned a non-uniform frequency spectrum, that can be estimated during the calibration process, the following relationship can be extracted,

$$\sigma_n = \sqrt{\frac{1}{N^2}\sum_{j=0}^{N-1}|H_j|^2} \tag{10}$$

Redundant measurements are an effective way to reduce the effect of noise. If the noise is assumed Gaussian with zero mean and standard deviation σ_n, an effective way to reduce it is increasing the number of measurements N. Then, since the system is linear we can just take it into account substituting the measurements with their mean values, and the noise will reduce with a factor $\frac{1}{\sqrt{N}}$,

$$\tilde{\psi} = \frac{1}{N}\sum_l \psi_l \Rightarrow \frac{1}{N}\sum_l(\psi_l + h * \zeta_l) = \tilde{\psi} + \frac{h}{N} * \sum_l n_l = \tilde{\psi} + \frac{h}{\sqrt{N}} * \zeta \tag{11}$$

A similar conclusion can be drawn, when the number of measurements is multiplied by a factor N, for the ratio $\frac{f_n}{f_p}$ (defined later), which can be proved to reduce by a factor $\frac{1}{\sqrt{N}}$. More details on the treatment of noise can be found in Oppenheim et al. [22].

3 Inverse procedure

The inverse procedure presented aims at characterizing damage in a structure and determine its extent (degree of degradation) and location. The testing consists of two steps: (1) to disturb a structure with a known excitation function (usually an impact loading simulated by a delta function) and (2) to measure its response (transient time history or a waveform representing the displacements, usually obtained by accelerometers) at one or more locations in the structure.

Then, the measured signal is processed to solve the *inverse problem*, i.e., to determine the changes in the structure from its original state. A genetic algorithm search tool [7,15] is used to minimize the discrepancy between the experimental readings and the numerically predicted trial response, by means of a cost functional designed to calibrate for coherent uncertainties and noise, and providing maximal robustness and sensitivity. Thus, we focus on determining the best cost functional for detecting damage from responses with noise. We propose and optimal choice of measuring points as well as time windows and wavelet level filters for better sensitivity to noise effects. The criterion for this is chosen in a rational way so as to maximize the probability of detection.

3.1 Cost functional

The readings from the sensors are denoted by ψ for the theoretical or synthetic case, and ψ^x for the experimental

case. A different magnitude called measurement Φ is defined to be analyzed instead of the readings ψ. The reason is to improve the measurement by converting it to a calibrated magnitude, so that it gains independency from the ambient conditions during the experiment and coherent noise, and also by being adimensional. A reading $\overset{\circ}{\psi}$ in the undamaged state of the specimen is defined for calibration, and the measurement to analyze is defined as the linear relationship,

$$\Phi = \frac{\psi - \overset{\circ}{\psi}}{RMS(\overset{\circ}{\psi})} \tag{12}$$

where the RMS values are defined for a discrete function f in time domain $f(t_i)$ or frequency domain $F(\omega_j)$ at N sampling points as,

$$RMS(f) = \sqrt{\frac{1}{N}\sum_{i=0}^{N-1} f(t_i)^2} = \sqrt{\frac{1}{N^2}\sum_{j=0}^{N-1} |F(\omega_j)|^2} \tag{13}$$

A **residual** γ is defined from the misfit or **discrepancy** $\Phi^x - \Phi$ between the experimental measurements Φ^x and the synthetic ones Φ. The synthetic measurements are computed assuming that the dynamic behavior of the structure in its intact and damaged states is predictable using a well-calibrated model. A **filter w** is included, which is in general a time-dependent vector, and will be later defined for optimizing the residual,

$$\gamma = \mathbf{w} * (\Phi^x - \Phi) \tag{14}$$

The **cost functional** f or fitness function is defined after a residual vector γ of size N_γ as the quadratic form,

$$f = \frac{1}{2}|\gamma|^2 = \frac{1}{2}\frac{1}{N_\gamma}\sum_{i=1}^{N_\gamma} \gamma_i^2 \tag{15}$$

It is useful to define an alternative version of the cost functional denoted as f^l, with the property of improving the sensitivity while approaching the optimum, just by introducing a logarithm and a small value ϵ to ensure its existence. This definition particularly enhances the convergence speed when the minimization is tackled by with genetic algorithms or other random search algorithms (see Rus et al. [6]),

$$f^l = \log(f + \epsilon) \tag{16}$$

The **parametrization** can be defined within the subject of inverse problems as a characterization of the sought information (i.e. damage extent and location) with a reduced set of variables. The parameters are denoted by a vector $\mathbf{p}$ of length N_p. The vector of parameters that best describes the real defect is denoted by $\tilde{\mathbf{p}}$. In this case, a simple parameterization is used, consisting of three parameters per defect: the x and y position of the damaged area and its extent $1-\beta$, where β is the stiffness reduction factor,

$$\mathbf{p} = \{x_1,\ y_1,\ 1-\beta_1,\ x_2,\ y_2,\ 1-\beta_2, \ldots\} \tag{17}$$

At this point, the **inverse problem** of defect evaluation can be stated as a minimization problem, that can be constrained, as finding $\mathbf{p}$ such that,

$$\min_{\mathbf{p}} f^l(\mathbf{p}) \tag{18}$$

3.2 Probability of detection

Three variables are be considered in the problem of maximizing the probability of detection (POD), the level of noise, denoted by σ_n, the location and extent of the defects, denoted by $\mathbf{p}$, and the cost functional that collects the effects of those in a scalar function $f(\mathbf{p}, \sigma_n)$, as defined above.

In this procedure, the case of one simultaneous position for the defect is assumed. A damaged specimen with a small but finite defect $\tilde{\mathbf{p}} = \mathbf{p}$ is tested, and it is assumed that the measurements contain no noise ($\sigma_n = 0$). Two cost functionals $f(\mathbf{p}, \sigma_n)$ are evaluated, one for the correct parameter $\tilde{\mathbf{p}}$ and another without defect $\mathbf{p} = 0$ (referring in the sequel to the extent parameters, i.e. $\beta = 1.0$), a measure for the rate of variation of the range of values of f with respect to some magnitude of the defect can be defined as $f_{,\mathbf{p}}$, considering the quadratic nature of the cost function, which is just a consequence of the definition of the cost functional as a least squares of the residual in Eq.(15),

$$f_{,\mathbf{p}} = \frac{d^2 f}{d\mathbf{p}^2} = \lim_{\mathbf{p}\to 0} 2\frac{f(\mathbf{p},0) - f(0,0)}{\mathbf{p}^2} \tag{19}$$

For a larger defect $\mathbf{p}$, that cost functional without noise effects will be called f^p, and can be approximated by the former, taking into account that $f(0,0) = 0$,

$$f^p = f(\mathbf{p},0) = 0 + \frac{1}{2} f_{,\mathbf{p}} \mathbf{p}^2 + hot. \tag{20}$$

If an undamaged specimen ($\tilde{\mathbf{p}} = 0$) is tested with noise σ_n, the evaluation of one each functionals with and without noise provide an approximation for its rate of variation with the ammount of noise, $f_{,n}$, in a similar

formulation, where the index n refers to noise (not to be confused with the time step mentioned earlier),

$$f_{,n} = \frac{d^2 f}{d\sigma_n^2} = \lim_{\sigma_n \to 0} 2\frac{f(0,\sigma_n) - f(0,0)}{\sigma_n^2}$$
$$f^n = f(0,\sigma_n) = 0 + \frac{1}{2} f_{,n}\sigma_n^2 + hot. \tag{21}$$

The ratio between those derivatives gives the linearized (first order) approximation of the relationship between the amount of noise and the size of the defect, which is a function of the position of the defect, and the ratio $\frac{\mathbf{p}}{\sigma_n}$ becomes independent of the form of the cost function f,

$$\frac{f^p}{f^n} \simeq \frac{f_{,\mathbf{p}}}{f_{,n}} \left(\frac{\mathbf{p}}{\sigma_n}\right)^2 \tag{22}$$

The *POD* is now defined as the probability that the alteration of the cost functional by the defect is larger than the effect of the noise on that cost functional, $POD = P(f^n \leq f^p)$. If the noise is assumed to be a stochastic process with a normal distribution, and since f is a sum of $N_m N_t$ squares of normal processes (N_m is the number of measurements and N_t is the number of time steps when time is discretized), it holds a $f^n \to \alpha\chi^2$ distribution (see Rade [24]) with the number of degrees of freedom $D = N_m N_t$ and α a multiplicative constant. The χ^2 distribution can be approximated, if $D > 10$, by a Gaussian distribution $N(\mu,\sigma)$ with mean $\mu = D - 2/3$ and $\sigma = \sqrt{2D}$.

If f^n is evaluated a single time, it tends to the mean value μ' of its random process $f^n \to \alpha N(\mu,\sigma) = N(\tilde{\mu},\tilde{\sigma})$. This allows to approximate the value of α, and hence,

$$\alpha = \frac{f^n}{D - 2/3} \Rightarrow \tilde{\mu} = \alpha\mu = f^n,$$
$$\tilde{\sigma} = \alpha\sigma = f^n \frac{\sqrt{2D}}{D - 2/3} \tag{23}$$

Provided that the probability is $P(z \leq x) = \alpha = F(x)$ and $F(x) = \int_{-\infty}^{x} f(y)dy$ is the normal cumulative distribution function with zero mean and standard deviation $\sigma = 1$, whose inverse is $x = G(\alpha) = G(F(x))$, the *POD* is,

$$POD = P(f^n \leq f^p) = F\left[\frac{f^p - \tilde{\mu}}{\tilde{\sigma}}\right]$$
$$POD \simeq F\left[\frac{D - 2/3}{\sqrt{2D}}\left(\frac{f_{,\mathbf{p}}}{f_{,n}}\left(\frac{\mathbf{p}}{\sigma_n}\right)^2 - 1\right)\right] \tag{24}$$
$$\frac{\mathbf{p}}{\sigma_n} \simeq \sqrt{\frac{f_{,n}}{f_{,\mathbf{p}}}\left(1 + G[POD]\frac{\sqrt{2D}}{D - 2/3}\right)}$$

The maximization of the POD is therefore equivalent to the minimization of $\frac{p}{\sigma_n}$, and in the case of several possible defect positions, a *minimax* criterion (pessimistic) is introduced to ensure that no defects are left undetected,

$$\max POD \quad \Leftrightarrow \quad \min\left(\max_{\text{position}} \frac{\mathbf{p}}{\sigma_n}\right) \tag{25}$$

3.3 Optimization of filters

A generic filter $\mathbf{w}$ was introduced in the definition of the cost function f to improve its sensitivity to the damage and its robustness against noise. It should be highlighted that the formulation is completely generic for any choice of the design of the filter $\mathbf{w}$, and would not need to be defined at this point. However, we may advance that, in this proposal, the filter is composed by three superposed filters: one to select a time window, another for selecting the levels of the wavelet decomposition, and another one for selecting a set of measurement points.

The filters $\mathbf{w}$ are optimized with the criterion of maximizing the POD. The benefit of this is that certain selections provide more sensitivity to the defect and less sensitivity to the noise, while others provide the opposite, which would damage the overall quality of the information available from the readings.

Figure 2 illustrates a flow chart for the optimization of the filters $\mathbf{w}$ computed by the finite element analysis and genetic algorithms, as applied in this study. Using the optimal $\mathbf{w}$ computed as shown, the location and extent of damage is finally determined by running the second stage of the flow chart.

4 Numerical examples

4.1 Numerical model

A composite plate of dimensions 0.5 × 0.5 m and thickness 5 cm is tested. The boundary conditions are clamped on two opposite sides as shown in Fig. 3. An impact force is applied at the marked point, and measurements are made at the 15 points distributed over a regular 3 × 5 mesh. The impact load has a magnitude of 10 MPa and a duration of 0.1 ms, whereas the measurement recording period is 1 ms.

Some assumptions are made for the simulation of the impactor and the receiver. The signals generated by the impactor are described by prescribing the pressure boundary conditions $q_i(x,t)$. The validity of this assumption was studied by Rus et al. [25] by comparing the results between the two extreme cases of Neumann and Dirichlet boundary conditions. This stress is assumed to

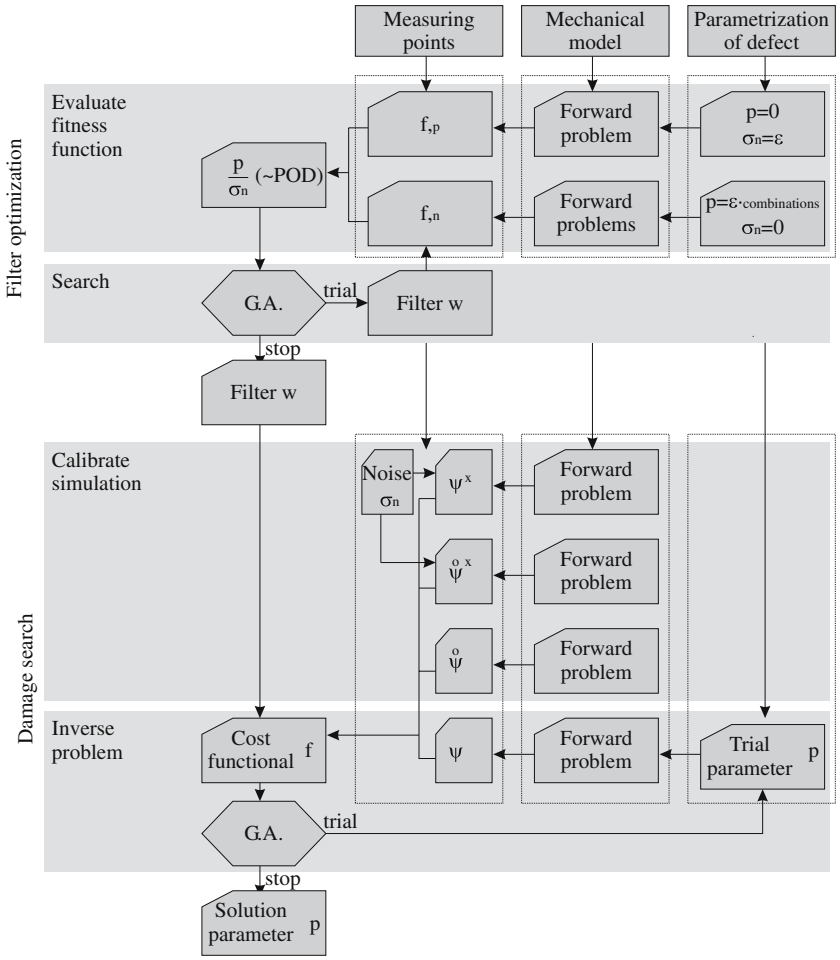

Fig. 2 A flow chart for determining (1) the optimal filter **w** using genetic algorithms and (2) for determining location and extent of damage using the optimal filter **w**. The chart is understood by starting from the information at the top, which corresponds to the definition of the problem, and follows the *arrows* to every box, that represents the computation of some data, which is explained in the text. They are grouped in categories by horizontal bands

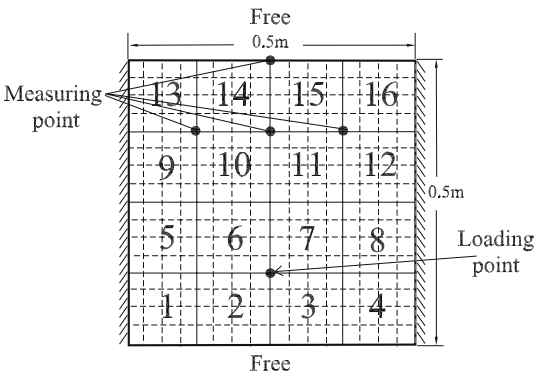

Fig. 3 Numerical model of the laminated composite plate divided into 16 zones

be distributed uniformly over the area of contact. Thus, the impact pressure can be prescribed by multiplying the constant pressure q_i and its phase or time delay $\varphi(t)$,

$$q_i(x,t) = q_i\varphi(t). \tag{26}$$

The output signal from the receiver is assumed to be the time average of displacements u_i of the points on Γ_n, the area of contact between the specimen and the receiving transducer. Shear stresses cannot be sustained on the specimen-impactor or the specimen-receiver boundaries, which means that only normal components of displacements u_i are taken.

$$u_i(t) = \int_{\Gamma_n} u_i(\Gamma,t)d\Gamma. \tag{27}$$

In order to determine optimal mesh size and time step for the FEM, the estimated errors are computed for different mesh refinements and time steps, as shown in Fig. 4. It can be observed that the combination of a time step of 0.01 ms and a mesh discretization in 16×16 elements gives an error sufficiently below 2%.

Figure 5 shows the deformed shapes for different time steps of composite plates with undamaged and damaged areas. The damage is defined as a $1-\beta = 50\%$ reduction over the area $m = 7$ (β =0.5). The differences are more clearly observed at the left and right boundaries of the plate at instants $t = 0.44$ ms and $t = 0.72$ ms. Table 1 presents the estimated wave speeds for different layup sequences at damaged and undamaged conditions. It

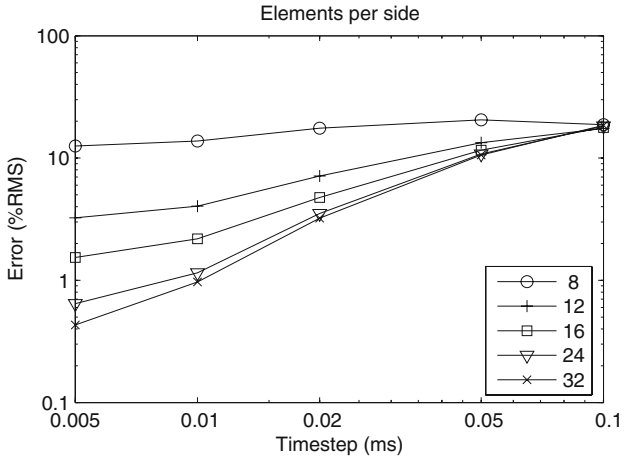

Fig. 4 Evolution of estimated relative error (%) in the forward problem for different time steps and divided mesh numbers of a $[90°/0°]_s$ composite plate. This error is defined as the average over the adimensionalized errors on every degree of freedom, whose real value is estimated by a highly refined solution

can be observed from the table that the wave speeds are significantly different for symmetric and antisymmetric cases. The wave speeds are measured as a group velocity from the delay of two wave cycles, which is estimated by the difference between the first and the fifth local extrema, as depicted in Fig. 6. This represents the velocities required for the propagating elastic wave originated by the impact to travel the distance between the loading and detection points. We can observe from the table that the speed of antisymmetric laminates in both directions is faster than that of the symmetric laminates except for $[90°/15°]$. For the $[0°/15° \sim 45°]$, the wave speed of undamaged plate is faster than that of damaged case. By contrast, the $[0°/45° \sim 90°]$, the wave speeds show reverse trends in the both directions. On the other hand, the reverse results for the $[\theta°/0°]$ are predictable because the angles of the laminate are orthogonal to $[\theta°/0°]$. The wave propagation speed of laminates for the different fiber angles is a dominant characteristic in identifying damages of composite from impacting.

4.2 Optimal damage detection

4.2.1 Optimal filtering

As mentioned above, in this proposal, the filter **w** is composed by three superposed filters: one for the time window, which is defined by cubic interpolation from

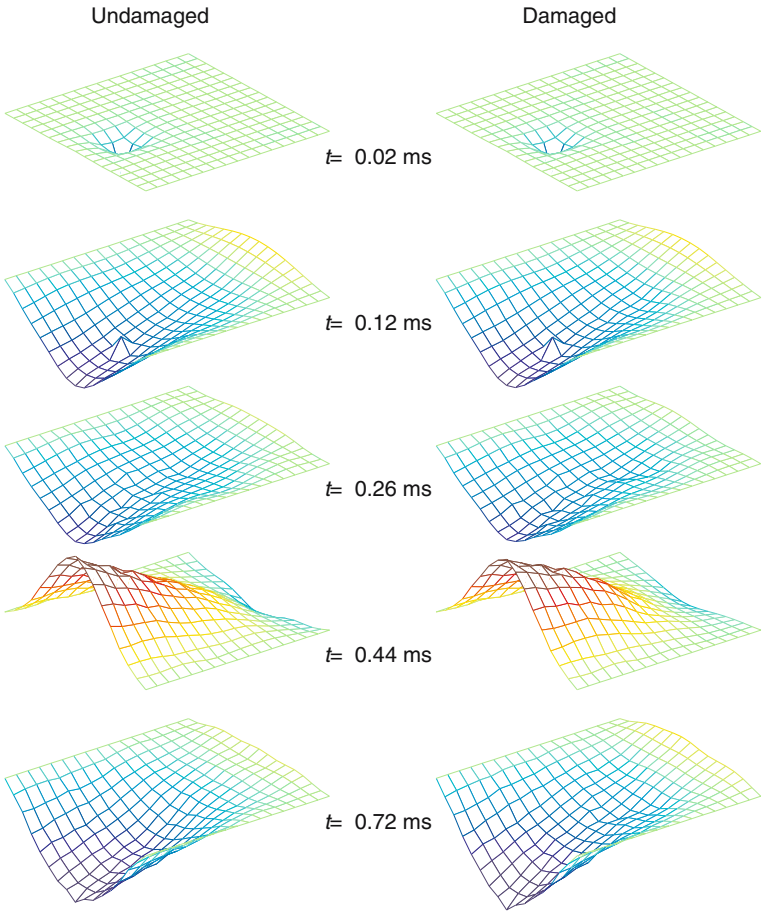

Fig. 5 Deformed shapes at different time steps of $[90°/0°]_s$ laminates with undamaged and damaged areas. The subscript s denotes symmetric layup sequence. In this case, $[90°/0°]_s$ means a symmetric laminate with cross-ply four layers $[90°/\,0°/\,0°90°]$

Table 1 Estimated wave speeds (m/s) for different layup sequences at damaged and undamaged conditions. The subscript 2 means unsymmetric layup sequence

	X direction		Y direction	
Angle	Undamaged	Damaged	Undamaged	Damaged
$[0°/15°]_s$	1912.78	1898.25	2990.43	2986.85
$[0°/15°]_2$	1911.31	1899.69	2990.43	2990.43
$[0°/30°]_s$	1915.71	1906.94	2944.64	2944.64
$[0°/30°]_2$	1929.01	1924.55	3015.68	3019.32
$[0°/45°]_s$	1930.50	1930.50	3378.38	3378.37
$[0°/45°]_2$	1956.18	1965.41	3373.82	3369.27
$[0°/60°]_s$	1923.08	1937.98	2682.40	2693.96
$[0°/60°]_2$	1988.86	1980.98	3511.23	3531.07
$[0°/75°]_s$	1909.85	1920.12	2759.38	2765.48
$[0°/75°]_2$	2034.17	2012.88	3140.70	3090.23
$[0°/90°]_s$	1909.85	1912.78	2074.69	2071.25
$[0°/90°]_2$	2057.61	2030.86	3059.97	3022.97
$[90°/0°]_s$	1776.83	1794.69	2876.87	2870.26
$[90°/0°]_2$	2057.61	2030.87	3059.97	3022.97
$[90°/15°]_s$	1783.16	1792.11	2860.41	2860.41
$[90°/15°]_2$	1511.49	1509.66	3041.36	3019.32
$[90°/30°]_s$	1612.90	1603.59	2834.47	2834.46
$[90°/30°]_2$	1815.54	1564.45	2997.60	2983.29
$[90°/45°]_s$	1209.48	1204.24	2799.55	2796.42
$[90°/45°]_2$	1378.93	1382.74	2934.27	2930.83
$[90°/60°]_s$	2133.10	2122.24	2765.48	2759.38
$[90°/60°]_2$	2240.14	2226.18	2831.25	2824.85
$[90°/75°]_s$	2122.24	2102.60	2759.38	2753.30
$[90°/75°]_2$	2145.92	2127.66	2765.49	2759.38

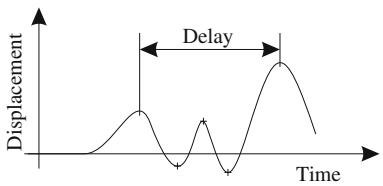

Fig. 6 Definition of the delay measurement procedure to estimate the group velocity from the time-delay between wavefronts

five points with values 1 or 0; another for five levels of the `rbio6.8` wavelet decomposition, also with 1/0 values; and another for selecting a fixed number of measurement points out of the 15 possible ones described in the geometry. A discrete wavelet decomposition of the measurement is introduced in order to separate the detail levels in the signal amplitude and the time dimension. If the wavelet transform of a function $WT(f)$ provides a set of detail coefficients $c(t_i, l)$, $i = 1 \dots N_t$, $l = 1 \dots N_l$, they allow to recover the original signal by their inverse transform $f(t_i) = IWT(c(t_i, l))$ together with some approximation coefficients. A `rbio6.8` wavelet is used throughout, since it empirically appears to provide a better sensitivity. This wavelet is the Reverse Biorthogonal wavelet of order 6 for decomposition and order 8 for recomposition. The detail coefficients can be used for defining the weighting filter $\mathbf{w} = \{\mathbf{w}_m, \mathbf{w}_i, \mathbf{w}_l\}$ by the composition of three filters $\mathbf{w}_m$ to select the measurement, $\mathbf{w}_i$ to select the time window (that is defined for few points and then oversampled), and $\mathbf{w}_l$ to select the detail level, as

$$\mathbf{w}(f_m(t_i)) = IWT(\mathbf{w}_m \mathbf{w}_i \mathbf{w}_l c_m(t_i, l)) \tag{28}$$

The ratio $\mathbf{p}/\sigma_n$, which gives a relative measure of the size of the defect that can be detected, and therefore an indication of the probability of detection. An example of the wavelet decomposition is given on Fig. 7. It should

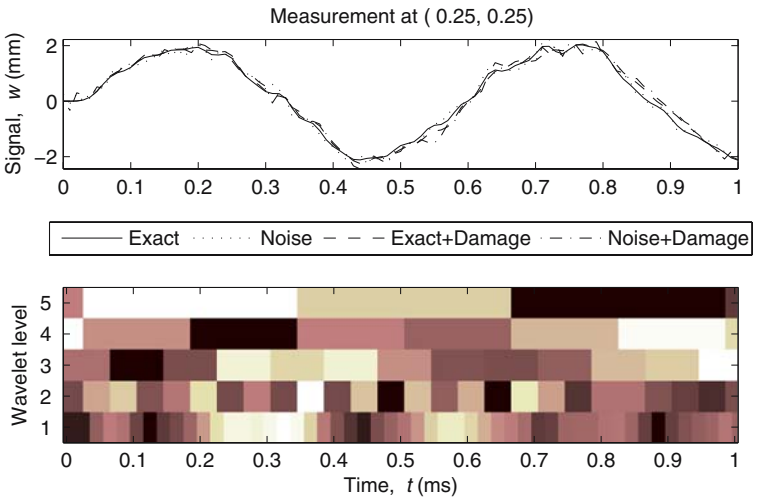

Fig. 7 Residual for a single measurement (above: the signals are close to each other since the effect of the damage is small, an also comparable to the effect of noise), and its wavelet decomposition into coefficients (represented by *shades* of *gray*) at several levels

be remarked from this figure and Fig. 5 that the effect of the damage on the waveform is not only small but also significantly masked by the effect of 10% noise, which is the reason of the difficulty of identifying the damage.

Now, a standard GA is implemented for the search of the defect and the optimal filter. This is done first by considering the time windowing, the selection of measurement points and the wavelet level. The characteristic parameters for tuning the GA are a crossover fraction of 0.6 and a migration fraction of 0.4. The number of generations is 100, and the number of individuals in the population is 30. Bitstring coding is preferred instead of real coding after empirical evidence. For the optimization of the POD, the term f_p/f_n is approximated by finite differences using $\epsilon_n = 1\%$ and $\epsilon_p = 6.25\%$. These values fall empirically within a wide range of finite difference steps that does not affect significantly the final value of f_p/f_n.

The wavelet level and time window optimization is performed with the minimum possible number of bits to represent the combination of measurement points, 5 bits for the five wavelet levels and 5 bits for the five reference points in time. An example of this filter optimization is given in Fig. 8. The ratio $\mathbf{p}/\sigma_n$ is represented for each case. This ratio is proportional to the extent of the minimum damage that can be found, and inversely proportional to the allowed noise level. This means that the lower $\mathbf{p}/\sigma_n$, the better is the probability of detection. The upper figure shows the sequential values of the ratio $\mathbf{p}/\sigma_n$ as the three filters are applied, as well as the value of the filter. The lower figure combines the three former optimizations simultaneously, giving a slightly different result that in the sequential case. In this case, a binary coding is used with the sum of the former number of bits.

As pointed out by Rus et al. [8], note that from the previous experience and from the examples above, there do not seem to be simple rules for the optimum collocation of sensors, but the improvement in the probability of detection is important.

4.2.2 Damage search

Figure 9 studies the effect of the number of defects as well as the effect of the optimization of the weight filter on the search of a single defect. The figure represents a map with the value of the cost functional when a trial defect is tested on each of the 4×4 possible damaged areas, using the correct value of it. A noise of $\sigma_n = 0.1$ (10%) is included in all cases. In the search procedure, a binary coding has been also adopted, with a phenotype defined with 8 bits for one defects and 16 for two, in which 2 bits define the horizontal position, 2 bits the vertical, and 4 bits the damage factor, which allows a range of 16 different values. The use of the optimum filter improves the contrast between the cost functional on the correct and incorrect trial points, which is indirectly a reason for improving the POD. It is observed that the overall value of the cost functional also decreases and is smoother, which also contributes to the numerical convergence of the search, and reduces the risk for falling in false local minima.

Finally, in the case of optimal filtering, the genetic algorithms almost fully recover the location and extent of the defect despite the noise of 10%, whereas without filter, a larger discrepancy arises in the identified parameters. This shows that the optimum filter not only allows to increase the probability of detection (consequently either to reduce the minimum size of the defect to be detected or conversely to increase the allowed level of

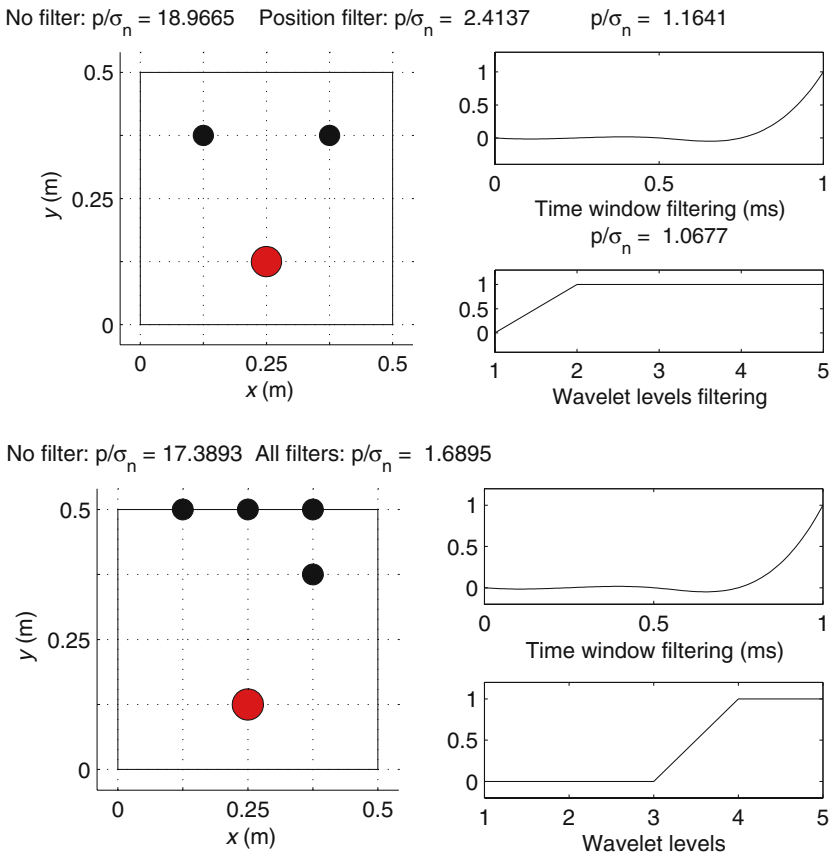

Fig. 8 *Above*: sequential optimization of the measurement point filter, the time window filter and the wavelet levels filter. *Below*: simultaneous optimization of the three filters. Cases of 2 (*top*) and 4 (*bottom*) measurement points respectively, and a layup $[90°/0°]_{1S}$ in both cases. The *dark* and *shaded* points denote measuring and loading locations, respectively

noise), but also reduces the discrepancy between the identified and real parameters.

4.3 POD for different filters

The *POD* is estimated from a simulation of the noisy signal to estimate the mean noise effect f_n and the effect of all the 4×4 possible defects f_p processed from Eq. (24). The results are shown in Fig. 10 for the case of no weight filter, wavelet filter, position filter and optimum combined filter respectively, to show the improvement. An increase factor around 6 is observed in the size of the minimum damage that can be detected if the optimum filter is applied. This improvement is even significant if a partial filter is applied. The best gain is achieved through the measuring position filter. This relative improvement factor highlights the performance of the main contribution of this paper, namely the optimum filter **w**.

5 Effect of layup sequences

Figures 11 and 12 show the $\mathbf{p}/\sigma_n$ ratio for different fiber angles of laminates. The lower values of $\mathbf{p}/\sigma_n$ means that the search is sensitive to smaller damages under higher noise. We can observe from the figures that antisymmetic cases are lower values of $\mathbf{p}/\sigma_n$ than those of symmetric cases. This can be explained that the coupling term B_{ij} for the antisymmetric laminate makes positive influnece on detecting the degradation of stiffness. In the figures, it can be also observed that $[45°/\theta°]$ and $[30°/\theta°]$ laminates present lower $\mathbf{p}/\sigma_n$. By contrast, the p/σ_n of $[\theta°/90°]$ and $[\theta°/15 \sim 30°]$ laminates show unpredictable trends for detecting the degradation of stiffness. It may be noted from the figures that the fiber angle of a laminate is a significant factor in identifying the degradation of stiffness. This conclusion is compatible with that obtained by Rus et al. [26].

Figure 13 shows the interaction between $\mathbf{p}/\sigma_n$ and the number of layers (same thickness) for different layup sequences. We can observe that the $\mathbf{p}/\sigma_n$ decreases for the increased number of layers except for $[45°/-45°]$ laminate. This phenomenon indicates that increased layers result in better damage detection.

Figure 14 shows the detection of the stiffness degradation for different thickness-length ratio (h/l) of symmetric and antisymmetric laminated composites. As the thickness-length ratio increases, the $\mathbf{p}/\sigma_n$ presents a stable trend especially for small fiber angles. This is predictable because the induced displacement becomes

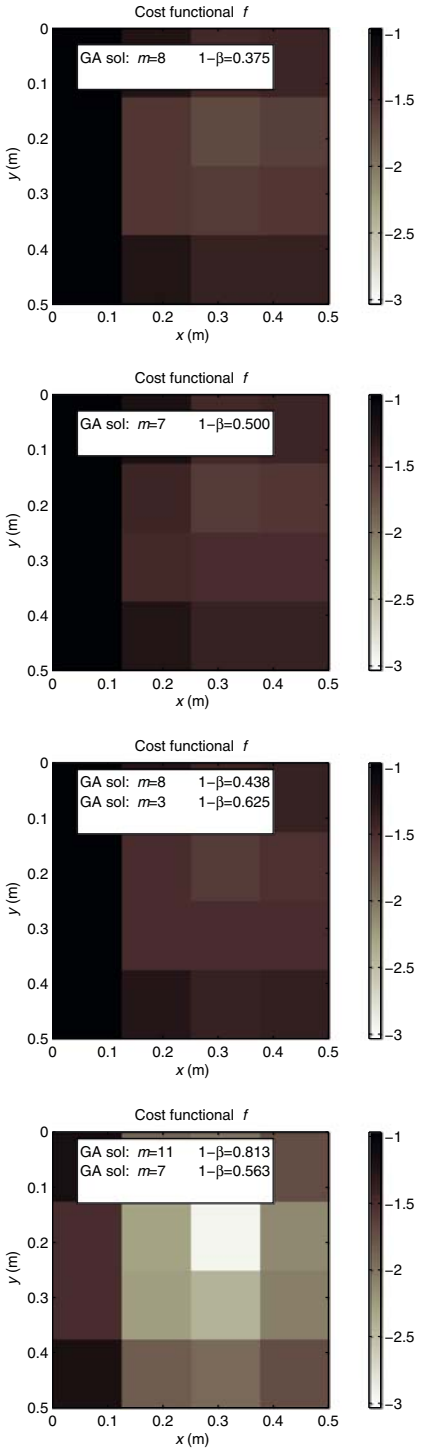

Fig. 9 Search of single and two damages. The *gray* scale colors represent the values of the cost functional f^l. From *top* to *bottom*, plots 1,3: without weight filter; plots 2,4: with optimum filter. Plots 1,2: case of 1 damage, whose real parameters are $m = 7$, $1 - \beta = 0.50$; plots 3,4: case of 2 damages, whose real parameters are $m = 7$, $1 - \beta = 0.50$ and $m = 15$, $1 - \beta = 0.75$ (the x and y coordinates represent the position the first damage, assuming the second is correctly located). Note that zone $m = 1$ is the one starting at coordinates $x = 0.0$, $y = 0.0$. Case of 4 measurement points and a layup $[90°/0°]_1$

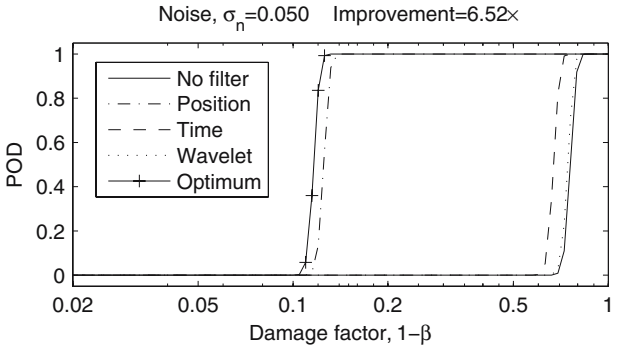

Fig. 10 Probability of detection without filtering and with filtering. Case of 4 measurement points and a layup $[90°/0°]_{1S}$

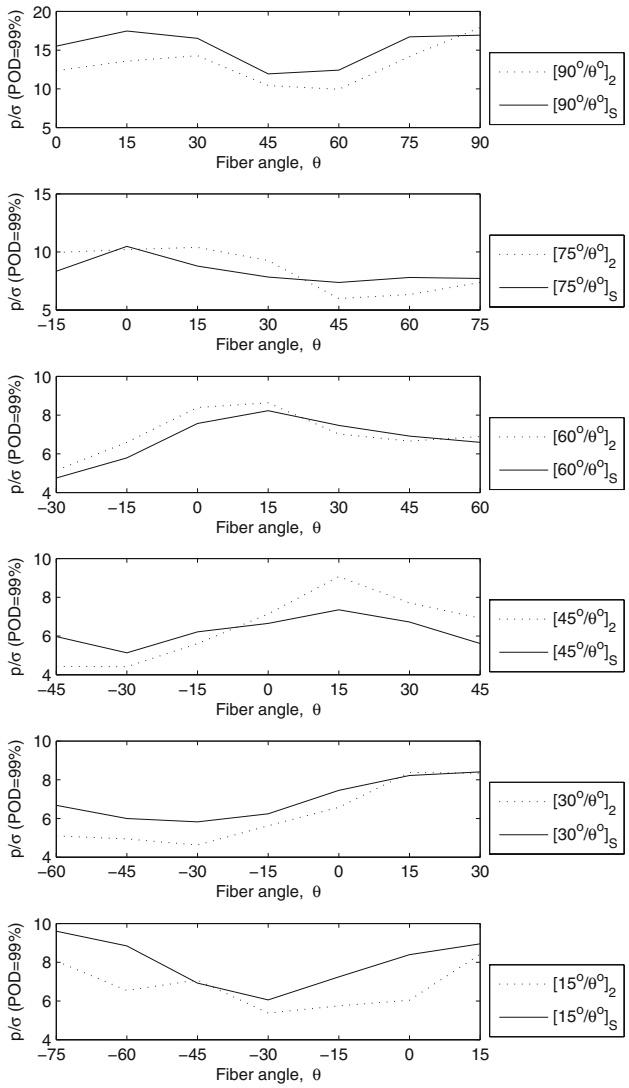

Fig. 11 Variation of the fiber angle θ at the second layer. *Continuous lines*: symmetric laminates; *discontinuous lines*: unsymmetric laminates

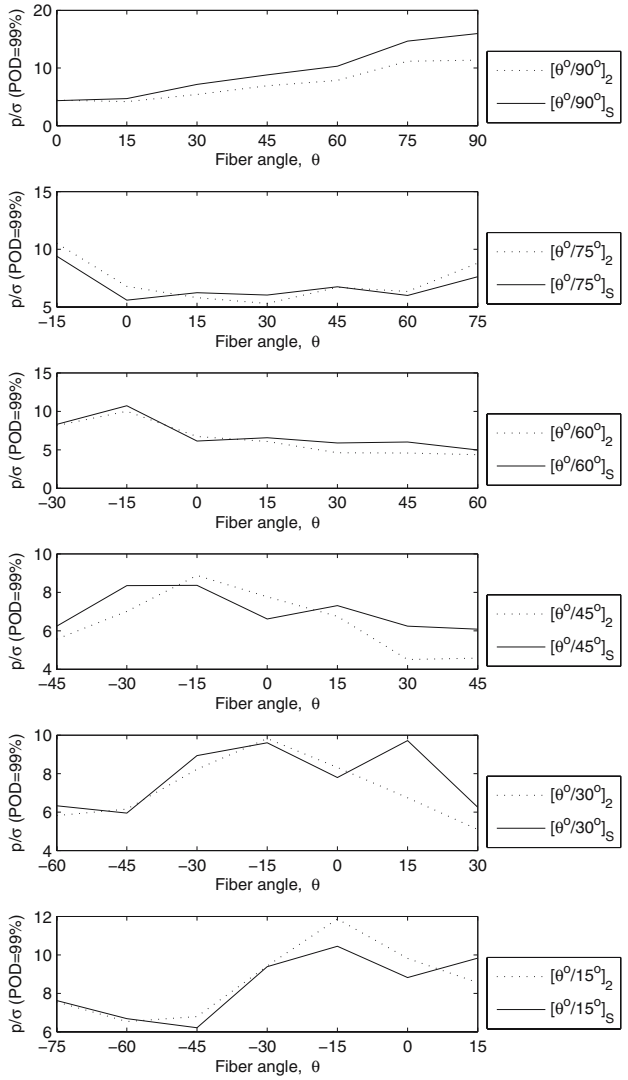

Fig. 12 Variation of the fiber angle θ at the second layer. *Continuous lines*: symmetric laminates; *discontinuous lines*: unsymmetric laminates

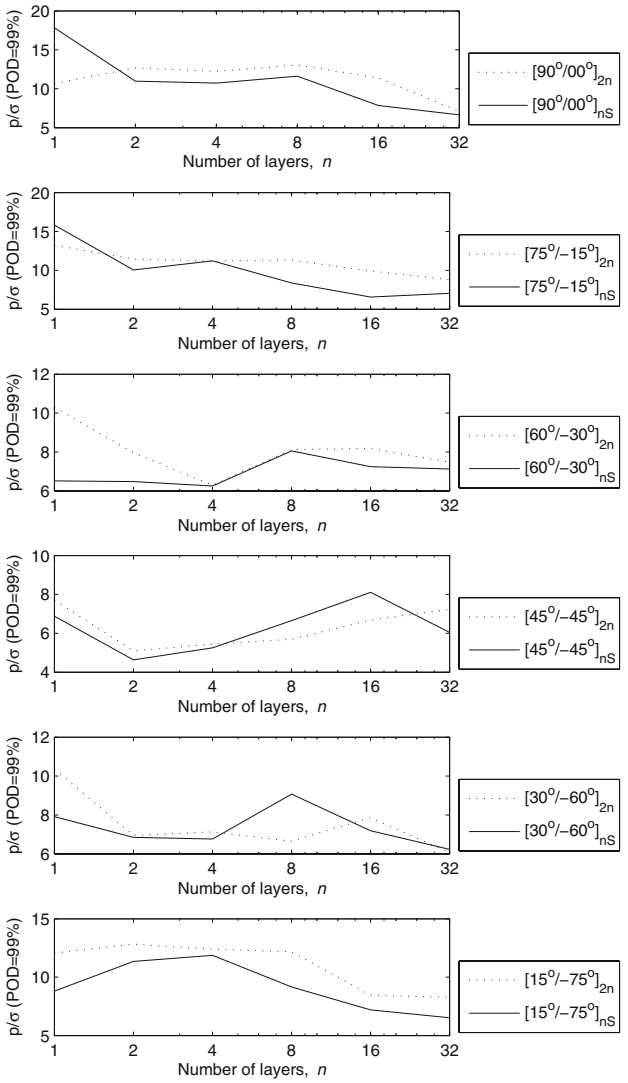

Fig. 13 Variation of the number of layers *n*. *Continuous lines*: symmetric laminates; *discontinuous lines*: unsymmetric laminates

constant for the increased thickness-length ratio. The constant displacement results from the effect of transverse shear deformation based on the FSDT. However, we may pay attention to the fact that the values of h/l less than 0.05 and $[45°/-45°]$ laminate are sensitive to the detection of stiffness degradation.

6 Conclusions

This paper presents a technique to improve the processing of the recordings from impact testing in a generalized inversion scheme, for the case of composite laminates. A filter is introduced in the definition of the damage characterization cost function to improve its sensitivity to the damage and its robustness against noise. It has three components: one to select a time window, another for selecting the levels of a wavelet decomposition, and another one for selecting a set of measurement points. All these data are optimized with the rational criterion of maximizing the *POD*. In the numerical tests, the use of this optimal filter provides an increase factor around 6 in the size of the minimum damage that can be detected. The optimum filter not only allows to increase the probability of detection, but also reduces the discrepancy between the identified and real parameters, and the proposed methods allow to easily characterize damage under noise levels of 10%.

An finite element analysis is carried out for simulating the dynamic response of composite laminate plates based on FSDT, where the effect of the layup sequence design, number of layers and thickness for improving

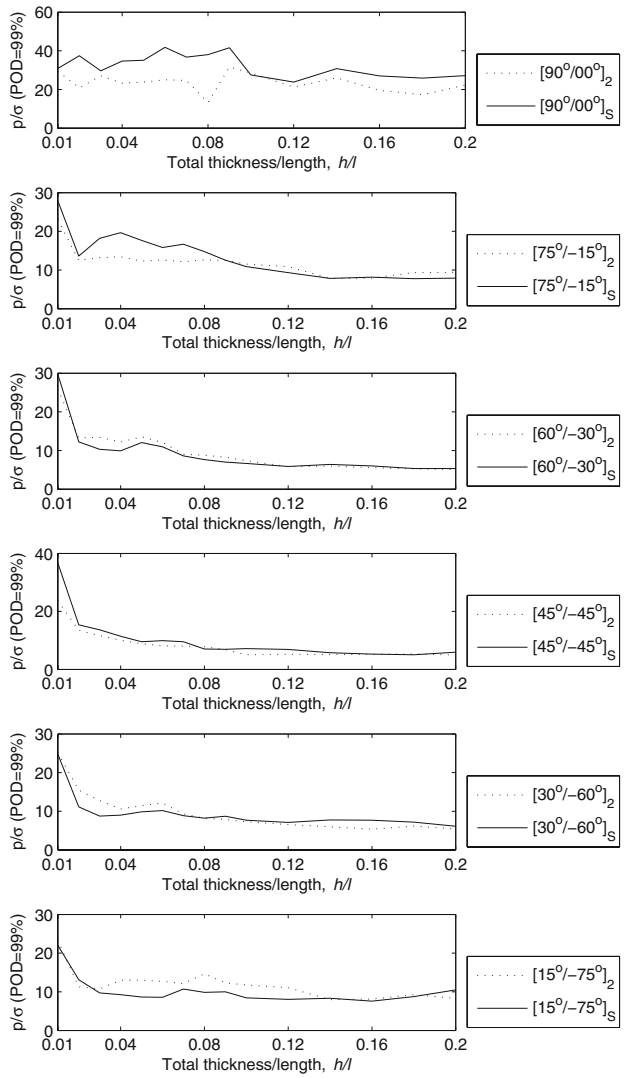

Fig. 14 Variation of the total thickness. *Continuous lines*: symmetric laminates; *discontinuous lines*: unsymmetric laminates

the *POD* is studied. Among the relevant conclusions, it can be noted that antisymmetic cases provide better *POD* than those of symmetric cases; the sensitivity to damage detection is better as the number of layers increase; and that this also happens for thin plates with thickness–length ratios less than 0.05.

It is concluded from this study that the approach works well for the numerical tests, especially for complex structures such as anisotropic composite plates. Even under the consideration of noisy effects in the measurements, the proposed method is useful for detecting the stiffness degradation. However, in order to prove the effectiveness of the technique for real-life situations, it will be necessary to prove the concept from experimental studies using a more detailed damage model.

References

1. Addison P (2004) The little wave with the big future. Phys World March:35–39
2. Au FTK, Cheng YS, Tham LG, Bai ZZ (2003) Structural damage detection based on a micro-genetic algorithm using incomplete and noisy modal test data. J Sound Vib 259(5):1081–1094
3. Bathe KJ (1996) The finite element procedures in engineering analysis. Prentice Hall, Englewood Cliffs
4. Chou JH, Ghaboussi J (2001) Genetic algorithms in structural damage detection. Comput Strut 79:1335–1353
5. Friswell M, Pennyb J, Garvey S (1998) A combined genetic and eigensensitivity algorithm for the location of damage in structures. Comput Struct 69:547–556
6. Gallego R, Rus G (2004) Identification of cracks and cavities using the topological sensitivity boundary integral equation. Comput Mech 33:154–163
7. Goldberg D (1989) Genetic algorithms in search, optimization and machine learning. Addison-Wesley, Reading
8. Han SC, Lee SY, Rus G (2005) Postbuckling analysis of laminated composite plates subjected to the combination of in-plane shear, compression and lateral loading. Int J Solids Struct (in press)
9. Kideir AA, Reddy JN (1988) Dynamic response of antisymmetric angle-ply laminated plates subjected to arbitrary loading. jsv 126(3):437–445
10. Kim IK, Kim YY (2005) Damage size estimation by the continuous wavelet ridge analysis of dispersive bending waves in a beam. J Sound Vib (in press)
11. Krawczuk M (2002) Application of spectral beam finite element with a crack and iterative search technique for damage detection. Finite Elem Anal Des 38:537–548
12. Kreja I, Schmidt R, Reddy JN (1997) Finite elements based on a first-order shear deformation moderate rotation theory with applications to the analysis of composite structures. IJ Non-linear Mech 32(6):1123–1142
13. Kumar A, Shrivastava RP (2005) Free vibration of square laminates with delamination around a central cutout using hsdt. Comp Struct 70(3):317–333
14. Lee SY, Wooh SC (2005) Detection of stiffness reductions in laminated composite plates from their dynamic response using the microgenetic algorithm. Comput Mech 36: 320–330
15. Lee SY, Wooh SC (2005) Waveform-based identification of structural damage using the combined fem and microgenetic algorithms. J Struct Eng ASCE 131(9):1464–1472
16. Lee SY, Yhim SS (2004) Dynamic analysis of composite plates subjected to multi-moving loads based on a third order theory. ijss 41:4457–4472
17. Li B, Chen X, Ma J, He Z (2004) Detection of crack location and size in structures using wavelet finite element methods. J Sound Vib 285:767–782
18. Liu PL, Chen CC (1996) Parametric identification of truss structures by using transient response. J Sound Vib 191(2):273–287
19. Mares C, Surace C (1996) An application of genetic algorithms to identify damage in elastic structures. J Sound Vib 195:195–215
20. Messina A (2004) Detecting damage in beams through digital differentiator filters and continuous wavelet transforms. J Sound Vib 272:385–412
21. Oh J, Cho M, Kim JS (2005) Dynamic analysis of composite plate with multiple delaminations based on higher-order zigzag theory. ijss 42(23):6122–6140

22. Oppenheim AV, Schaffer RW (1989) Discrete-time signal processing. Englewood Cliffs, New Jersey
23. Pagano NJ (1970) Exact solution for rectangular bidirectional composites and sandwich plate. J Comp Mater 4: 20–34
24. Rsde L, Westergren B (1999) Mathematics handbook for science and engineering. Springer, Heidelberg
25. Rus G, Wooh S, Gallego R (2004) Analysis and design of wedge transducers using the boundary element method. J Acous Soc Am 115:2919–2927
26. Rus G, Lee S, Gallego R (2005) Defect identification in laminated composite structures by bem from incomplete static data. Int J Solids Struct 42:1743–1758
27. Suh MW, Shim MB, Kim MY (2000) Crack identification using hybrid neuro-genetic technique. J Sound Vib 238(4):617–635
28. Tarantola A, Valette B (1982) Inverse problems = quest for information. J Geophys 50:159–170
29. Yang WX, Hull JB, Seymour MD (2004) A contribution to the applicability of complex wavelet analysis of ultrasonic signals. NDT&E Int 37:497–504